I&EC research
Industrial & Engineering Chemistry Research

pubs.acs.org/IECR

Article

Experimental and Modeling Studies of Sr^{2+} and Cs^{+} Sorption on Cryogels and Comparison to Commercial Adsorbents

Alzhan Baimenov, Fabio Montagnaro, Vassilis J. Inglezakis,* and Marco Balsamo*

Cite This: *Ind. Eng. Chem. Res.* 2022, 61, 8204−8219

Read Online

ACCESS | Metrics & More | Article Recommendations | Supporting Information

ABSTRACT: In this work, two cryogels with the key monomers methacrylic acid and 2-acrylamido-2-methyl-1-propansulfonic acid (named AAC and SAC, respectively) with various functional groups were used as adsorbents for the removal of cesium and strontium ions from aqueous solutions. Kinetics, equilibrium, and column studies were carried out including experiments in different water matrices (ultrapure, tap, and river water) and comparison to commercial adsorbents. AAC reached sorption capacity of 362 mg g^{-1} for Cs^{+} and 209 mg g^{-1} for Sr^{2+}, whereas SAC polymer showed maximum removal capacities of 259 and 211 mg g^{-1} for Cs^{+} and Sr^{2+}, respectively. The five cycles of adsorption/desorption experiments showed a maximum of 8% loss of effectiveness for both cryogels. Batch kinetics adsorption data were modeled by using a rigorous diffusional model coupled to a novel fractal-like expression for variable surface diffusivity. The model revealed that the surface diffusivity dependence on time is nonmonotonic, with the occurrence of a maximum. Also, both fluid film and intraparticle transport resistances were shown to be important, with the internal one being more influential. The cryogels and two commercial materials (ion-exchange resin and zeolite) were tested for the removal of Cs^{+} and Sr^{2+} in ultrapure, tap, and river water; the results showed that the cryogels exhibit competitive effectiveness.

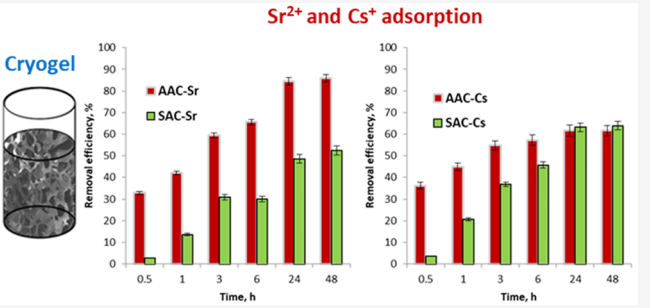

1. INTRODUCTION

With the growth in energy consumption, the development of alternative energy sources is becoming increasingly popular. Despite several advantages of nuclear power, its use is not risk-free, and accidents can be detrimental to people and the environment such as what happened in Chernobyl and Fukushima.[1] Among the harmful radionuclides leaked from nuclear power plants accidents, radioactive cesium (^{137}Cs) and strontium (^{90}Sr) have substantial toxic effects, emitting beta-particles and γ-rays. Moreover, due to the chemical similarity of ^{137}Cs and ^{90}Sr to K and Ca, respectively, the isotopes released after a nuclear accident can be easily incorporated into terrestrial and aquatic organisms. Both Cs and Sr radioisotopes have half-lives around 30 years; therefore, it is imperative to immediately and effectively remove them from wastewater and contaminated water bodies.[2]

Removal of radioactive ions from wastewater has been the focus of numerous studies.[2−6] Several methods have been considered for the recovery of metal ions from wastewater including chemical precipitation,[7] chemical coagulation/flocculation,[8] membrane filtration,[9] ion-exchange processes,[10] bioremediation,[11] and adsorption.[12] Typical adsorbents such as activated carbons (AC), natural zeolites, and clays have been used, but they are often characterized by low adsorption capacities or the need to be chemically treated to acquire desirable adsorption properties.[13−15] Natural sorbents like zeolites and AC usually show low removal capacities in the ranges of 1.3−10 mg/g for Sr^{2+} ions and 0.7−51 mg g^{-1} for Cs^{+}. Synthetic polymers like hydrogels and cryogels can reach much higher removal capacities, up to 312 mg g^{-1} for Sr^{2+} and 420 mg g^{-1} for Cs^{+} ions.[1,4,16−33] A list of literature works investigating Cs^{+} and Sr^{2+} ions adsorption from aqueous media onto different sorbents is reported in Table S1.

Certain properties are desirable when it comes to an effective cation adsorbent, e.g., (i) the presence of chelating sites or ion-exchange groups, (ii) a hydrophilic and three-dimensional (3D) network structure to uphold water-flow for an extended period of time, (iii) cost-effectiveness, (iv) facile synthesis, and (v) easily regeneration. Natural materials, like zeolites or charcoals, are low-cost, but without additional modification, they are nonselective and may have low removal efficiencies. Among several synthetic materials, cryogels are highly effective sorbents toward heavy metals ions.[34,35] Upon appropriate modification, the functional groups in their network structures, such as carboxyl (−COOH), hydroxyl (−OH), amine ($-NH_2$), and/or thiol (−SH), can provide the

Received: February 15, 2022
Revised: May 4, 2022
Accepted: May 19, 2022
Published: June 2, 2022

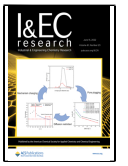

necessary chelating sites for effective cation removal from aqueous solutions. Further advantages include the ease of regeneration and biodegradation. Despite the large number of published studies investigating adsorption kinetics modeling for different adsorbent/adsorbate systems, most use empirical expressions, e.g., pseudo-first- or pseudo-second-order models, not suitable for studying the underlying mechanisms and mass transfer phenomena. Some studies apply simplified diffusion-based models not mirroring the complex mechanisms taking place during surface diffusion, for instance, the occurrence of nonmonotonic patterns of the surface diffusivity in the course of the sorption process.[36,37] In the case of adsorption onto cryogels, a limited number of papers apply rigorous dynamic models; for example, a rate constants distribution model also accounting for diffusion limitations was recently proposed to interpret Cu(II) adsorption on a polyethylenimine cryogel.[38] In the present paper, a detailed understanding of intraparticle transport mechanisms is gained by applying a diffusion-based model accounting for fluid film, pore, and surface transport of the adsorbate. In particular, the element of novelty in dynamic modeling relies in adopting our recently proposed fractal-based expression for surface diffusivity able to depict the above-mentioned nonmonotonic patterns in the time domain.[39]

In order to evaluate the impact of different functional groups on the removal of Cs^+ and Sr^{2+}, two different cryogels were synthesized by free-radical copolymerization of acrylate-based precursors with allylamine under subzero conditions. The first cryogel (AAC) is composed of copolymers of methacrylic acid, allylamine, dimethylacrylamide, and methylenbis(acrylamide). The second cryogel is allylamine-2-acrylamido-2-methyl-1-propansulfonic acid (SAC) and has a chemical composition of monomers and concentrations similar to those of AAC, but methacrylic acid is here substituted by 2-acrylamido-2-methyl-1-propansulfonic acid. The cryogels were fully characterized and applied for the removal of Sr^{2+} and Cs^+ ions from aqueous solutions. Kinetics and equilibrium studies were conducted, and dynamic adsorption results were interpreted by application of rigorous diffusion models including variable surface diffusivity expressions, a topic rarely investigated in the pertinent literature. The adopted fractal-like expression for the surface diffusivity allowed us to study the change of diffusivity during the adsorption process and quantitatively evaluate the relative importance of intraparticle versus fluid film mass transfer resistance. In combination with postsorption characterizations and obtained adsorption results, potential removal mechanisms were proposed. The effect of different water matrices and the comparison to commercial adsorbents were also studied. To the best of our knowledge, this work represents the most detailed experimental and modeling investigation for the removal of Sr^{2+} and Cs^+ ions by use of cryogels.

2. MATERIALS AND METHODS

2.1. Reagents. For the synthesis of cryogels, *N*,*N*-dimethylacrylamide (DMAAm, 99%), allylamine (AA) (98%), 2-acrylamido-2-methyl-1-propanesulfonic acid (AMPS), methacrylic acid (MAAc, 99%), *N*,*N*-methylenebis (acrylamide) (BisAAm, 99%), 70% H_3PO_4, 5 M NaOH, ammonium peroxodisulfate (APS, 98%), and *N*,*N*,*N*′,*N*′-tetramethyl ethylene diamine (TEMED, ≥99.5%) were used. $Sr(NO_3)_2$ and $CsNO_3$ (purity of 99%) salts were used as strontium and cesium sources for all adsorption experiments. All reagents were purchased from Sigma-Aldrich (Germany). Ultrapure water (UPW) purified by a Puris MR-RO1600 (Mirae ST, South Korea) reverse osmosis apparatus was used for the preparation of cryogels and metals solutions.

2.2. Synthesis of AAC and SAC Cryogels. Two cryogels with different compositions, named AAC and SAC, were synthesized at subzero temperatures by free-radical polymerization according to previously reported procedures.[40−42] Briefly, MAAc or AMPS for AAC and SAC cryogels, respectively, and the cross-linking agent BisAAm were mixed in 10 mL of preliminary degassed UPW and neutralized by 5 M NaOH. In another beaker, DMAAm and AA were added to 7.5 mL of UPW and acidified with concentrated H_3PO_4 under continuous stirring. Afterward, both solutions were intermingled and TEMED was added dropwise, followed by vigorous stirring and cooling in an ice bath for 30 min under N_2 atmosphere. After the cooling and degassing stages, 0.25 mL of 5 wt % of APS was added. Finally, 2 mL of the monomeric mixture was poured into plastic syringes of 1 cm diameter. Then, sealed syringes were placed in an ethanol cooled cryobath (Julabo F34, Germany) and kept at −12 °C for 24 h. The resulted monolithic cryogels were thawed out at room temperature and washed first with 10% ethanol and then with 2 L of UPW to remove unreacted reagents. For the further use, both types of cryogels were lyophilized on a FreeZone 2.5 L (Labconco, Kansas City, MO) instrument at −45 °C and under vacuum (0.4 mbar) for 48 h, in order to remove water.

2.3. Adsorbents Characterization. The morphological structure of cryogels coated by 7 nm Au was evaluated by using a Zeiss Crossbeam 540 scanning electron microscope (SEM) at 20 kV. Semiquantitative energy-dispersive X-ray (EDX) spectrometer (INCA X-sight, Oxford Instruments) connected to the SEM was used for characterizing point and surface elemental analysis before and after metal ions removal. For the determination of the cryogels structure by fluorescent confocal laser scanning microscope LSM 780 (Zeiss, Germany), the polymer discs were immersed in 0.5 M solution of rhodamine B for 24 h and then washed by water to remove dye from the polymer pores. Nitrogen adsorption/desorption experiments at −196 °C were carried out in an Autosorb IQ (Quantachrome Instruments, Ashland, VA) porosimeter to determine the cryogels textural properties. In particular, the micromesoporous surface area was evaluated according to Brunauer−Emmett−Teller (BET), Barrett−Joyner−Halenda (BJH), and Dubinin−Radushkevich (DR) models applied to raw adsorption data. Prior to the porosimetric analysis, lyophilized cryogel samples were degassed at 105 °C for 6 h to remove oxygen and humidity in pores. The X-ray photoelectron spectroscopy (XPS) measurements were conducted on a VG-Microtech Multilab 3000 device equipped with a 9-channeltrons hemispherical electron analyzer and X-ray radiation source with Mg and Al anodes. The binding energies (BE) were calibrated by a C 1s core level at 284.8 eV as a reference.

2.4. Adsorption Studies. *2.4.1. Effect of pH.* To assess the effect of pH on the adsorption efficiency of cryogels, a series of experiments was carried out in the pH range 1.0−5.0 at room temperature using 0.07 g of polymers in 100 mL of metal ion solutions with concentrations of 100 mg L^{-1}. The pH of Sr^{2+} and Cs^+ solutions with initial concentration of 100 mg L^{-1} was adjusted with HNO_3 to achieve the desired pH values. The residual concentrations of metal ions were analyzed by iCAP RQ ICP-MS analyzer (ThermoFisher Scientific, Waltham, MA).

https://doi.org/10.1021/acs.iecr.2c00531
Ind. Eng. Chem. Res. 2022, 61, 8204−8219

Table 1. Sorbents Textural Properties, D_m, and D_p Values Adopted as Input Parameters for the Dynamic Models

	textural parameters						
sorbent	R [m]	ε_p [−]	ρ_p [g m^{-3}]	adsorbate	D_m [m^2 s^{-1}][a]	sorbent/adsorbate	D_p [m^2 s^{-1}]
SAC	4.84×10^{-3}	0.85	4.38×10^{4}	Cs^+	2.06×10^{-9}	SAC/Cs^+	1.15×10^{-9}
						SAC/Sr^{2+}	8.81×10^{-10}
AAC	5.02×10^{-3}	0.89	3.95×10^{4}	Sr^{2+}	1.58×10^{-9}	AAC/Cs^+	1.31×10^{-9}
						AAC/Sr^{2+}	1.01×10^{-9}

[a]After Kadhim and Gamaj.[48]

The amount of adsorbed metal was calculated by material balance:

$$q_{eq} = \frac{(\overline{C_0} - C_{eq})V}{m} \quad (1)$$

The reader is referred to the "Nomenclature" section for the meaning of the symbols.

2.4.2. Batch Adsorption Kinetics. The Sr^{2+} and Cs^+ solutions were prepared by dissolving analytical-grade $Sr(NO_3)_2$ and $CsNO_3$ in UPW, respectively. A volume of 100 mL of a solution of Sr^{2+} and Cs^+ at 100 mg L^{-1} concentration was mixed without pH regulation (pH 5.5) with 0.07 g of cryogel in plastic tubes with shaking at 120 rpm at room temperature. At predetermined time intervals, a 0.1 mL sample volume was taken from the tubes and analyzed using ICP-MS (iCAP RQ, ThermoFisher Scientific, Waltham, MA) with the appropriate dilution. The total sampling volume in all experiments was kept below 3% of the original volume. Blanks with the same initial metal ion concentration and volume, without solids, were analyzed. Blank experiments showed that the loss of Sr^{2+} and Cs^+ due to adsorption on the tube walls was less than 2%. All experiments were carried out in duplicate; the experimental standard deviation was less than 5%. The specific amount of Sr^{2+} and Cs^+ adsorbed at each process time was calculated as

$$\overline{q(t)} = \frac{[\overline{C_0} - \overline{C(t)}]V}{m} \quad (2)$$

Batch kinetics data of Sr^{2+} and Cs^+ adsorption onto cryogels were modeled according to a rigorous diffusional model accounting for both pore volume and surface transport mechanisms, namely the pore volume surface diffusion model (PVSDM) as presented by Ocampo-Pérez et al.[43] The assumptions and equations of the PVSDM model are presented in the Supporting Information (eqs S1−S5).

Despite Langmuir and Freundlich equilibrium models allowing a general good interpretation of the whole adsorption isotherms (including equilibrium points at concentrations higher than those used for the batch kinetic run), a poor fitting of dynamic data for longer process times occurred when applying them as local isotherms to analyze the batch dynamic data. The equilibrium loading at low concentrations was generally underestimated by the above-mentioned models, thus resulting in unreliable dynamic transport parameters. As a consequence, the Henry model was selected as more adequate to describe local equilibrium at low concentrations, i.e., dilute liquid phase for the kinetics run modeling:

$$q(t, r) = K_H C_p(t, r) \quad (3)$$

The PVSDM was applied to analyze kinetic data by considering both a constant surface diffusivity D_s and expressions accounting for its variation along the adsorption process. In particular, the Chen and Yang's expression,[44] here abbreviated as CY (eq 4), and our recently proposed fractal-based equation, abbreviated as MBI in Inglezakis et al.[39] (eq 5), based on our previous works on the topic, e.g., Montagnaro and Balsamo[45] and Balsamo and Montagnaro,[46] were adopted:

$$D_s(\theta) = D_{s0}\frac{1 - \theta + \frac{\lambda}{2}\theta(2 - \theta) + H[1 - \lambda](1 - \lambda)\frac{\lambda}{2}\theta^2}{\left(1 - \theta + \frac{\lambda}{2}\theta\right)^2} \quad (4)$$

$$\frac{1}{D_s(t)} = \frac{1}{D_{s0}}\left[\frac{\beta}{(t + 1)^{-h}} + \frac{(1 - \beta)}{(t + 1)^{\alpha}}\right] \quad (5)$$

Both equations are characterized by a robust theoretical basis and, with respect to other expressions commonly found in the literature, they allow to predict increasing, decreasing and nonmonotonic patterns of the surface diffusivity. While the CY expression (eq 4) accounts for a D_s dependence on the surface coverage degree, $\theta = q(t, r)/q_m$, in the MBI expression (eq 5), the surface diffusivity is a function of the process time. In the following, the versions of the PVSDM including the CY and MBI equations are termed PVSDM-CY and PVSDM-MBI, respectively.

In order to compare the relative importance of intraparticle versus fluid film mass transfer resistance, the Biot number can be invoked.[47] In particular, for the analysis of the PVSDM-MBI case, we define in the present work an average Biot number $\overline{Bi(t)}$ as

$$\overline{Bi(t)} = \frac{k_f R \overline{C_0}}{\overline{D_s(t)}\rho_p \overline{q_0} + D_p \overline{C_0}} \quad (6)$$

where $\overline{D_s(t)}$ represents the mean integral value of the surface diffusivity function expressed by eq 5.

The solution of the partial and ordinary differential equations constituting the PVSDM, PVSDM-CY, and PVSDM-MBI, was carried out by adopting the method of lines implemented in the software MATLAB R2019b for the discretization of the particle radial coordinate. The best fitting parameters for the numerical models were determined by means of the *lsqnonlin* algorithm of MATLAB, which minimizes the sum of squared errors between experimental and theoretical values of pollutant concentration in the bulk solution. In order to reduce the number of fitting parameters for each model, the following numerical strategy was adopted at fixed sorbent/adsorbate system: (i) The k_f parameter was preliminary determined through fitting experimental data by means of the simpler homogeneous surface diffusion model, which accurately predicted adsorption data in particular in the first stages of the process, where fluid film resistance is more relevant. (ii) D_{s0} was fixed for both PVSDM-CY and PVSDM-MBI as the best fitting D_s value obtained from the application

https://doi.org/10.1021/acs.iecr.2c00531
Ind. Eng. Chem. Res. 2022, 61, 8204−8219

of PVSDM. Consequently, D_s was set as fitting parameter for PVSDM, λ for PVSDM-CY and the triad h, α, and β for PVSDM-MBI. Table 1 reports the sorbents textural properties, D_m values retrieved from literature for Sr^{2+} and Cs^+, and calculated D_p values, all adopted as input parameters for the numerical dynamic models. The relationship between D_m and D_p is provided in eq S4.

2.4.3. Equilibrium Adsorption Isotherms. A set of three equilibrium adsorption isotherms was obtained in batch mode without pH adjustment for each investigated adsorbate/adsorbent system. The difference among experiments is the use of various mass of cryogels and initial concentrations of Sr^{2+} and Cs^+, as shown in Table 2. All experiments were conducted in plastic tubes at least in duplicate under shaking, by use of a Rotamax 120 (Heidolph, Germany) at room temperature, by sampling and measuring the residual Sr^{2+} and Cs^+ daily until equilibrium was reached. The total liquid sampling volume was less than 3%. The average relative standard deviation for all experiments was 1.5%, while on graphs the absolute standard deviation values will be reported for each solid-phase loading.

Table 2. Parameters of Isotherm Adsorption Experiments

no. of experiment	mass of cryogels [g]	initial concentration [mg L^{-1}]	solution volume [mL]
1	0.0022−0.150	100	100
2	0.07	100−1000	100
3	0.07−0.9	1000	100

Since analytical errors are inevitable, it is necessary to take into account that if the difference between the initial and equilibrium concentrations of the adsorbate in the aqueous phase is not sufficiently large, then considerable errors and unreliable results may occur when calculating the equilibrium capacity of the sorbent. This is especially important when using a small amount of adsorbent and a large concentration of adsorbate. It was calculated that for a relative analytical concentration error of about 2.5% and a desired capacity relative error of less than 15%, the equilibrium concentrations of the aqueous phase should be kept below 85% of the initial concentration. To avoid significant uncertainties, this rule was followed in the present study.

The results of the experiment 2 were adopted to evaluate the fitting of experimental data with respect to the widely used Langmuir and Freundlich isotherm models, as expressed by eqs 7 and 8, respectively:[49]

$$q_{eq} = \frac{q_m K_L C_{eq}}{1 + C_{eq} K_L} \quad (7)$$

$$q_{eq} = K_F C_{eq}^{1/n} \quad (8)$$

The Langmuir sorption isotherm assumes the monolayer adsorption of adsorbate onto the homogeneous surfaces, while the Freundlich sorption isotherm corresponds to multilayer adsorption on energetically heterogeneous surface. The total release of Na^+ ions from both types of cryogels in metal-free solutions was evaluated by placing 80 mg of dry polymer in 100 mL of UPW under shaking at 120 rpm for 30 days. The investigated sodium release was around 1.3 mg g^{-1} for both cryogels.

2.4.4. Leaching Experiments. The release of the metal ions from the cryogels after adsorption was studied by leaching experiments at pH 6.5. Following the equilibrium experiments, the cryogel samples with the highest loading were washed with 1 L of UPW in tightly closed containers, and the systems were left for 30 days under shaking (120 rpm) at room temperature. The average BJH pore size is considerably smaller than this identified by SEM images, probably due to resolution limitations related to SEM. The samples were withdrawn from each container and analyzed for leached Sr^{2+} and Cs^+. All the leaching experiments were carried out in duplicate, and the average values are reported.

2.4.5. Removal from Various Water Matrices and Comparison to Commercial Adsorbents. Removal studies were conducted in batch mode by mixing 10 mg of each adsorbent with 50 mL of metal solution at 10 mg L^{-1}

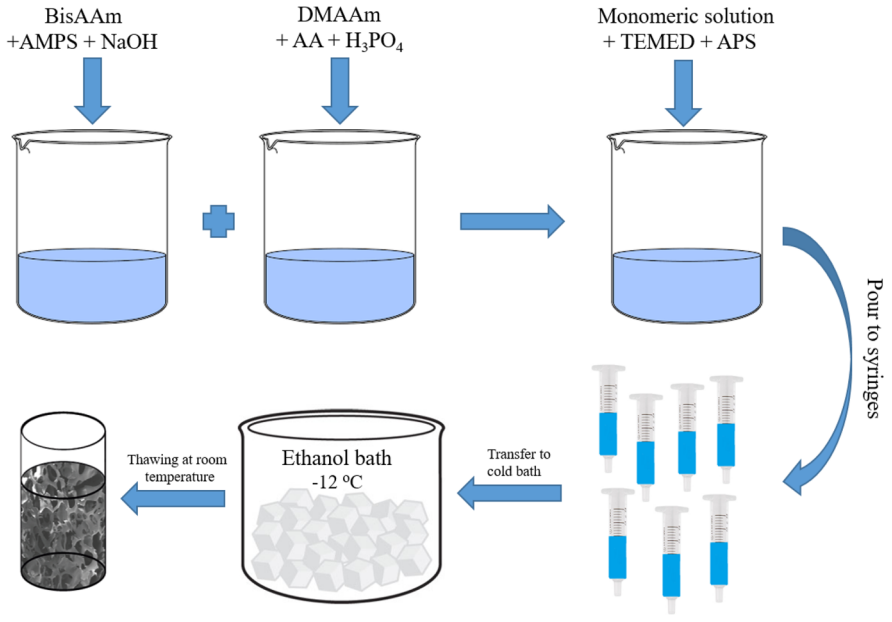

Figure 1. Schematic representation of the formation of SAC cryogel.

https://doi.org/10.1021/acs.iecr.2c00531
Ind. Eng. Chem. Res. 2022, 61, 8204−8219

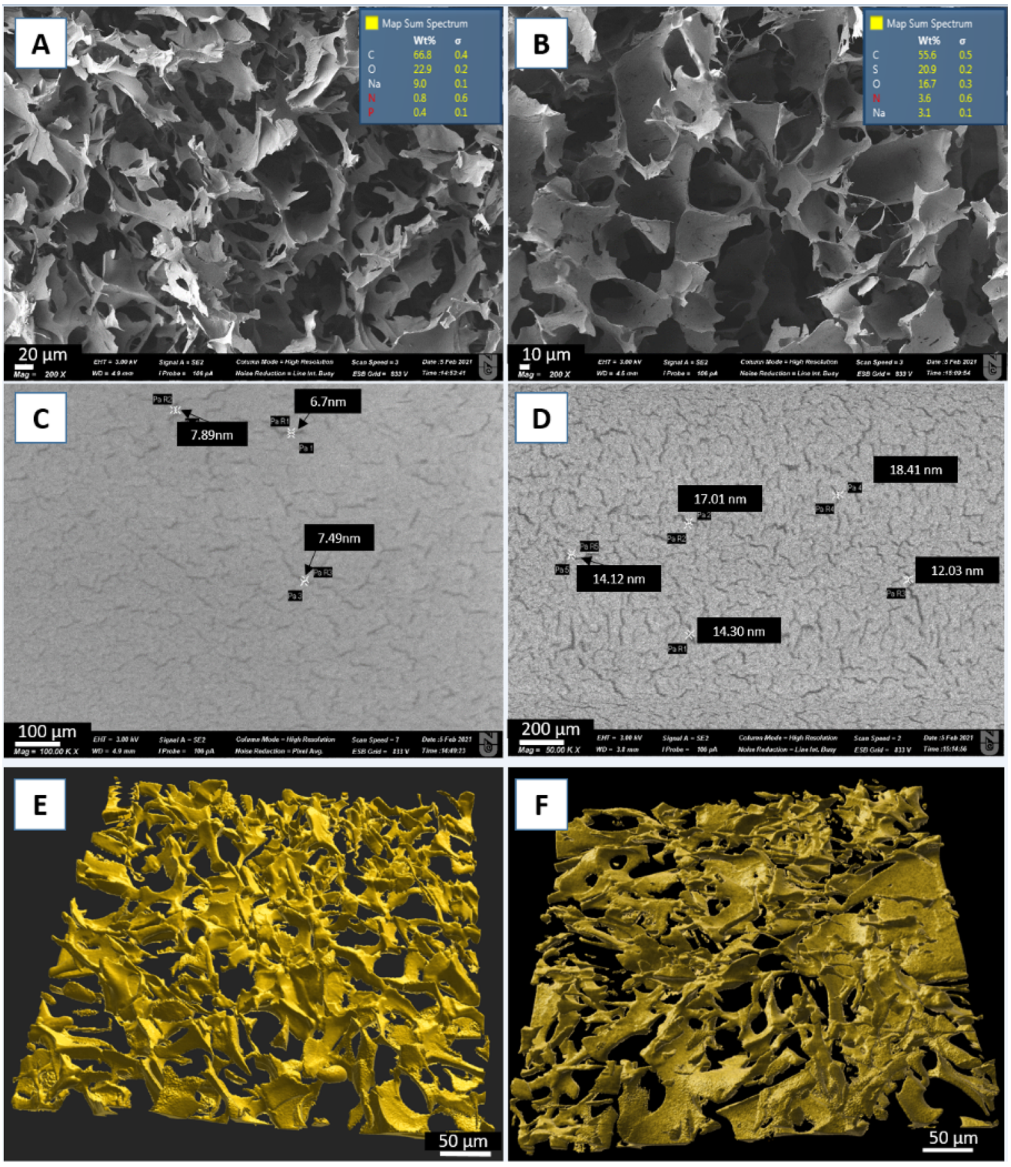

Figure 2. SEM, EDX elemental composition, and confocal microscopy images of the AAC (a, c, and e, respectively) and SAC (b, d, and f, respectively) cryogels.

concentration in different water matrices. UPW, tap water (from Nazarbayev University laboratories), and river water (sampled from 43°15′4.0″N 76°51′50.7″E, Bolshaya Almatinka, Almaty, Kazakhstan) were used without any further purification. The efficiency of cryogels were compared with commercial ion exchange materials, namely, an H^+-form ion-exchange resin (Merck) and NaY synthetic zeolite (Sigma-Aldrich). Sampling was done at 30 min and 2 and 24 h, and the residual Sr^{2+} and Cs^+ concentrations were measured by Dionex ICS 6000 ion chromatograph, after filtering through 0.45 μm hydrophilic filter and dilution. The experiments were done in duplicate, and the average values are reported.

2.4.6. Column Experiments. A dry cryogel monolith (1 cm height and 0.7 cm diameter) was placed into a plastic column (15 cm height and 0.8 cm internal diameter) and wetted with UPW. Upon contact with water, the cryogels diameter increased by 1 mm, and as a result, the monoliths adhered tightly to the column walls, which excludes the possibility of the passage of aqueous metal solutions between the cryogel and the column walls, i.e., bypass phenomena. A down-flow rate of 2.5 mL min^{-1} was maintained by using a peristaltic pump (Gilson, Minipuls 3). The experiments were carried out at room temperature, at 100 mg L^{-1} of Sr^{2+} and Cs^+ concentration. Samples were collected from the outflow every minute, and they were analyzed as described in the previous sections. Three simplified models, namely, Thomas', Yoon–Nelson's, and Adams–Bohart's models, were adopted to fit the breakthrough data. The models are presented in the Supporting Information eqs S6–S8.

2.4.7. Regeneration and Reusability of Cryogels. The monolithic samples of cryogels used for column studies, after interaction with metal ions, were washed by 10 mL of 0.1 M HCl to remove adsorbed pollutants. After recovery, the column experiments were repeated with cryogel under the same conditions as described above. Five consecutive cycles of regeneration/adsorption were carried out. After each regeneration, cryogels were washed with 50 mM NaOH and then UPW.

https://doi.org/10.1021/acs.iecr.2c00531
Ind. Eng. Chem. Res. 2022, 61, 8204–8219

Table 3. Microstructural Parameters of Cryogels

	BET	BJH			DR		
	specific surface area [m^2 g^{-1}]	specific surface area [m^2 g^{-1}]	specific pore volume [cm^3 g^{-1}]	pore diameter [nm]	specific micropore surface area [m^2 g^{-1}]	specific micropore volume [cm^3 g^{-1}]	pore diameter [nm]
AAC	62.34	45.44	0.167	4.27	60.77	0.022	3.09
SAC	147.38	165.06	0.230	3.06	112.09	0.040	3.04

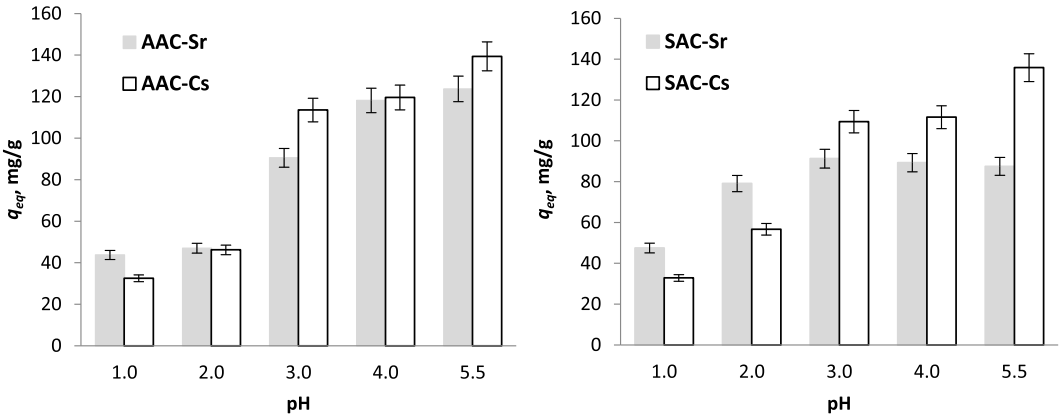

Figure 3. Equilibrium loading of metal ions (Sr^{2+} and Cs^{+}) by AAC (left) and SAC (right) cryogels at different pH values.

3. RESULTS AND DISCUSSION

3.1. Synthesis and Characterization of Cryogels. The schematic representation of cryogels formation via cryopolymerization technique is shown in Figure 1. To enhance the activity of allylamine and increase the yield of the gel fraction of copolymerized AMPS and AA, allylamine was converted to a phosphate complex by mixing with phosphoric acid.[50,51] Placing the monomeric solution at subzero temperatures initiates the growth of ice crystals, which occurs with radical polymerization of selected monomers, and the cross-linking of polymer chains to form branched macromers in unfrozen liquid microphase.[52] The size of the formed ice crystals depends on the temperature in the cryobath. Polymerization goes on until free monomers run out, or until termination of all radicals occurs. Upon completion of the polymerization reaction and ice thawing, a hollow of microcrystals leads to macro-sized pores development within the polymeric structure.

The structural morphology and formation of macropores of the cryogels was observed by scanning electron microscope. SEM images display a cross-linked polymeric network integrated with super-macropores with pore diameters of 10−50 μm (Figure 2a,b). While the general structure of cryogels is macroporous, the walls of polymers have slit-cylindrical micropores in a range of 5−20 nm (Figure 2c,d). The images of the three-dimensional structure of the swollen cryogels were evaluated by fluorescence confocal microscopy at a depth of 150 μm, and processed with Imaris Software. It is clearly seen that the whole structure of the AAC polymer shows homogeneous distribution of macropores (Figure 2e). The SAC cryogel has a more rigid and tight structure due to the presence of AMPS monomer (Figure 2f).

SEM/EDX analysis is often used for the determination of elemental composition of cryogels.[40,53] The mass percentage of carbon and oxygen were found to be in approximately the same level for the AAC and SAC cryogels. Since the amount of NaOH used in AAC cryogel synthesis was higher than that in the SAC sample: The mass percentage of Na in the final AAC was 9%, while in SAC it reached only 3.1%. In SAC cryogel, the main monomer was sulfur-containing AMPS, and the amount of sulfur in the adsorbent was equal to 20.9% (Figure 2a,b). The microporosities of the cryogel walls were also confirmed by the nitrogen adsorption/desorption porosimetry technique. The specific surface areas of cryogels were determined by a multipoint BET analysis, while the BJH and DR models were used to determine mesoporous and microporous surface areas, pore volumes, and pore diameters, respectively. The results of porosity determination are presented in Table 3. The BET surface area of AAC is 62.34 m^2 g^{-1}, a value about 60% smaller than the one obtained for SAC. Similarly, the specific micropore volume of AAC is almost half the one retrieved for SAC when applying the DR method. The results of surface area and pore volume measurements by BJH and DR methods are in line with SEM images (Figure 2c,d), where SAC, visually, has a higher amount of slit pores on the surface of polymer.

The presence of various functional groups in the cryogels was discussed in details in our previous papers.[40,52] Briefly, both AAC and SAC polymers show the existence of amide(I) and amide(II) groups due to the presence of pDMAAm and BisAAm reagents. Peaks of COO^{-} carboxyl groups of amino acid residues and nondissociated carboxylic groups were determined at 1390 and 1141 cm^{-1}, respectively. Due to existence of AMPS monomer in SAC cryogel, the characteristic frequencies of sulfonic acid, sulfoxide, sulfide, and C−S functional groups were found. The zeta potential measurements results presented in our previous work showed that surface charge of AAC cryogel is negative in a wide range of pH, from 3.4 to 9, due to the deprotonation of carboxyl groups.[52] A positive charge of AAC at pH below 3.2 is attributed to positively charged amino groups of allylamine. In the case of the SAC cryogel, the surface is negatively charged for the whole pH range due to the presence of permanently negative form of dissociated sulfonic acid, which is a strong acid. It can be also assumed that amino groups of allylamine

https://doi.org/10.1021/acs.iecr.2c00531
Ind. Eng. Chem. Res. 2022, 61, 8204−8219

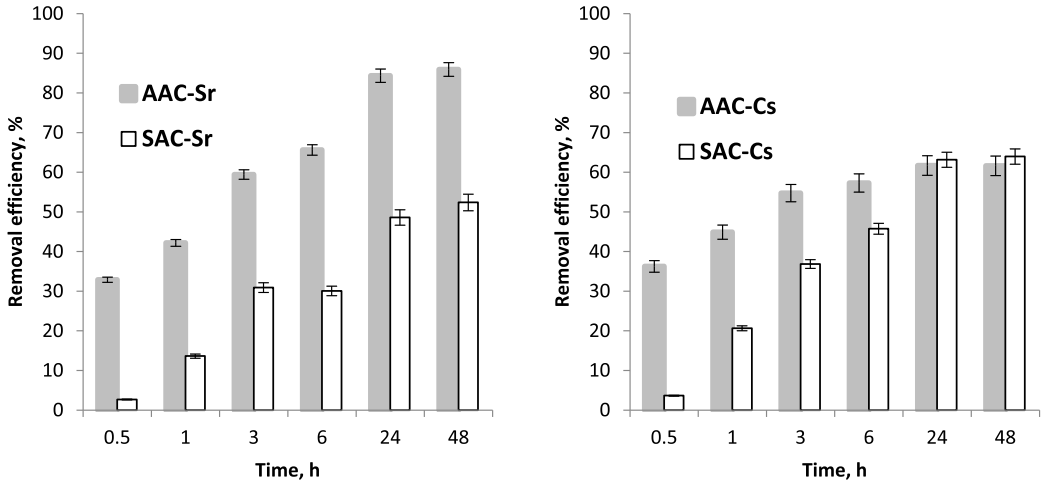

Figure 4. Removal efficiency of Sr^{2+} (left) and Cs^{+} (right) ions on the AAC and SAC cryogels (70 mg of cryogel in 100 mL of solution), at pH = 5.

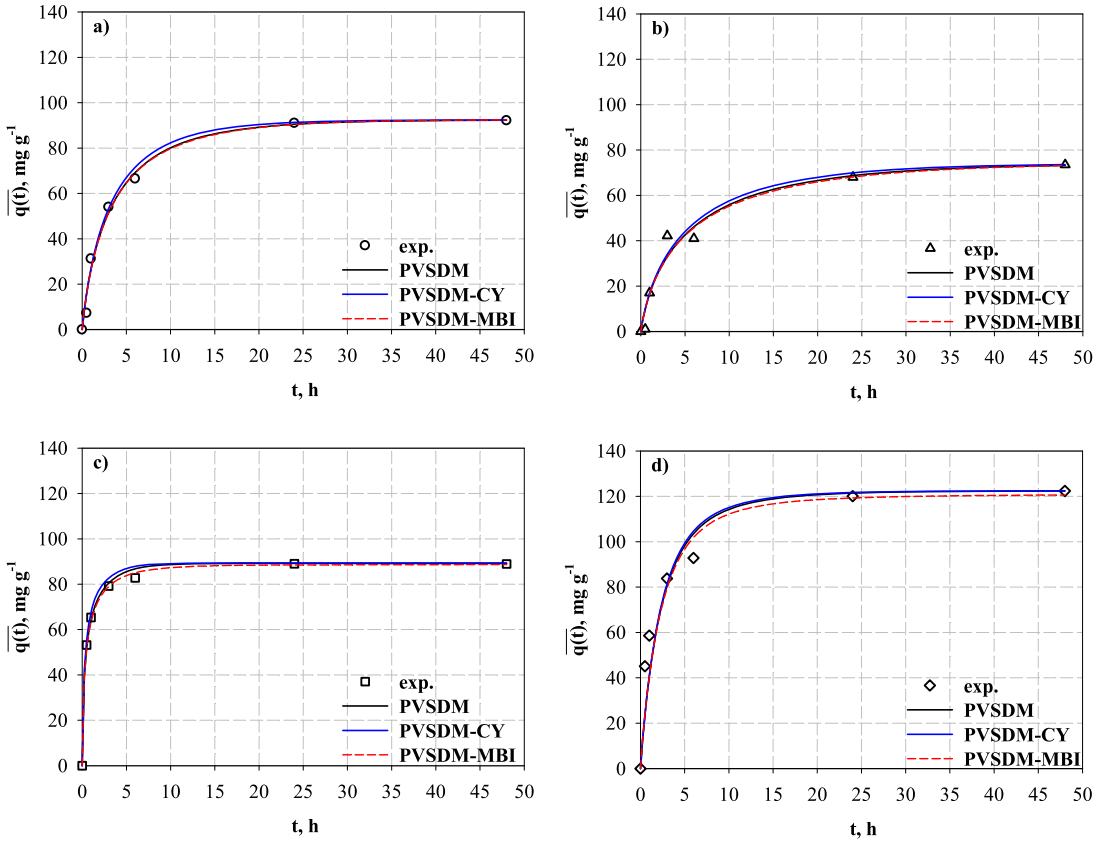

Figure 5. Comparison between experimental and theoretical kinetics adsorption patterns for the investigated sorbent/adsorbate systems: (a) SAC-Cs^{+}, (b) SAC-Sr^{2+}, (c) AAC-Cs^{+}, and (d) AAC-Sr^{2+}.

and neighboring sulfonic and carboxyl groups are protonated at low pH.[52]

3.2. Effect of pH on Metal Ions Adsorption. The pH of the solutions after the dissolution of 100 ppm Sr^{2+} and Cs^{+} ions of nitrate salt was around 5.5. To avoid the precipitation of these metal ions (in the form of insoluble hydrocomplexes), solution pH values of ≤5.5 was chosen for the experiments. Results of specific equilibrium adsorption capacity reported in Figure 3 show that the removal of strontium and cesium ions monotonically decreases with the diminution of pH. At a highly acidic pH value of 1.0, the adsorption capacities of the AAC and SAC samples for Sr^{2+} and Cs^{+} were around 44−47 and 33 mg g^{-1}, respectively. As the pH increased to 3.0, however, the removal efficiency doubled for Sr^{2+} and Cs^{+} ions, and the highest removal capacities of Sr^{2+} and Cs^{+} ions at pH 5.5 were 124 and 139 mg g^{-1} by AAC and 88 and 136 mg g^{-1} by SAC, respectively. At low pH, H^{+} competes for ion-exchange sites in the cryogel structure, hindering the uptake of metals.[52] Also, at higher pH values, excessive hydroxyl ions may cause a strong electrostatic attraction with the metal cations for the negatively charged adsorption sites, which causes sudden increases in adsorption capacity.

3.3. Adsorption Kinetics. The results of kinetics experiments are illustrated in Figure 4 in terms of removal efficiency

https://doi.org/10.1021/acs.iecr.2c00531
Ind. Eng. Chem. Res. 2022, 61, 8204−8219

Table 4. Main Parameters Determined from the Kinetic Modeling Campaign

	SAC-Cs^+	SAC-Sr^{2+}	AAC-Cs^+	AAC-Sr^{2+}
		PVSDM		
k_f [m s^{-1}]	8.56×10^{-6}	5.81×10^{-6}	1.55×10^{-4}	1.08×10^{-5}
D_s [m^2 s^{-1}]	5.00×10^{-11}	2.85×10^{-11}	1.76×10^{-10}	5.11×10^{-11}
R^2 [−]	0.9876	0.9650	0.9964	0.9187
		PVSDM-CY		
k_f [m s^{-1}]	8.56×10^{-6}	5.81×10^{-6}	1.55×10^{-4}	1.08×10^{-5}
D_{s0} [m^2 s^{-1}]	5.00×10^{-11}	2.85×10^{-11}	1.76×10^{-10}	5.11×10^{-11}
λ [−]	0.50	0.94	0.01	0.42
R^2 [−]	0.9863	0.9639	0.9924	0.9188
		PVSDM-MBI		
k_f [m s^{-1}]	8.56×10^{-6}	5.81×10^{-6}	1.55×10^{-4}	1.08×10^{-5}
D_{s0} [m^2 s^{-1}]	5.00×10^{-11}	2.85×10^{-11}	1.76×10^{-10}	5.11×10^{-11}
β [−]	0.25	0.12	0.24	0.11
h [−]	0.37	0.61	0.94	0.91
α [−]	0.20	0.20	0.84	0.47
$\overline{D_s(t)}$ [m^2 s^{-1}]	4.26×10^{-11}	2.29×10^{-11}	5.43×10^{-11}	2.87×10^{-11}
$\frac{\overline{D_s(t)}\,\rho_p \overline{q_0}}{D_p \overline{C_0}}$ [−]	1.58	0.79	2.55	1.74
$\overline{Bi(t)}$ [−]	13.98	17.83	166.92	19.66
R^2 [−]	0.9876	0.9651	0.9978	0.9204

as a function of process time. It is evident that the AAC sample shows a faster kinetics with respect to SAC sample in the removal of both cations in the first 8 h. In the first hour, AAC cryogel can remove about 42 and 45% of Sr^{2+} and Cs^+, respectively, while SAC removed only about 14 and 21%, respectively. After 24 h of contact with the strontium-containing solution, both cryogels reached equilibrium with removal efficiency values of 86% for AAC and 48% for SAC sample. In the case of Cs^+ ions, both AAC and SAC cryogels also reached equilibrium in 24 h with maximum removal efficiencies of 58 and 63%, respectively.

The presence of adsorbed Sr^{2+} and Cs^+ metal ions on the cryogels surface was verified by point EDX analysis and is presented in Figure S1. The overall picture of elemental analysis confirms that AAC cryogel has higher adsorption capability compared with SAC sample. The EDX analysis reveals that all adsorbed metal ions are evenly distributed over the entire surface of the polymers (see Figures S2−S5).

3.4. Kinetic Modeling Studies. The results of batch dynamic adsorption tests were modeled according to the theoretical framework described in section 2.4.2. Figure 5 reports a comparison between experimental and theoretical dynamic profiles of the adsorption capacity $\overline{q(t)}$ for the investigated systems, while Table 4 summarizes the main parameters determined from the modeling campaign. As a general observation, there are not very remarkable differences in the fitting accuracy of the three models. From close inspection of dynamic adsorption profiles and based on the R^2 values, it can be said that the diffusional model accounting for the Chen and Yang's expression for surface diffusivity (PVSDM-CY) exhibits slightly less fitting accuracy and tends to anticipate the attainment of equilibrium conditions with respect to experimental observations, for all the sorbent/adsorbate pairs. For both the SAC-Cs^+ and SAC/Sr^{2+} adsorption systems, both the diffusional model with constant surface diffusivity (PVSDM) and the fractal-based one (PVSDM-MBI) produce practically the same kinetics patterns. In the case of AAC cryogel and for both tested ions, the PVSDM-MBI shows a slightly superior ability in predicting $\overline{q(t)}$ versus time trends with respect to PVSDM. For each adsorbent material, Cs^+ exhibits faster sorption dynamics with respect to Sr^{2+}, as evidenced by greater values of k_f, D_p, and $\overline{D_s(t)}$ obtained for the former ion. This can be related to the greater value of molecular diffusivity of cesium with respect to strontium (see D_m in Table 1), which in turn is determined by a higher ionic mobility.[48] When comparing adsorbent materials for the same cation, faster sorption dynamics were observed for AAC cryogel when compared to SAC. The mass transfer coefficient in the fluid film is almost 20 times greater for AAC-Cs^+ with respect to SAC-Cs^+, while it is almost double for the AAC cryogel in the Sr^{2+} case. Similarly, the adsorbate transport in the AAC pores network is faster than in the SAC case (cf. D_p values in Table 1), which can be related to the slightly greater macroporosity of the AAC adsorbent (cf. ε_p in Table 1 and its favorable effects in eqs S4 and S5). The diffusion coefficients obtained for AAC and SAC cryogels was found in the range of 1.01×10^{-9}−8.81×10^{-10} m^2 s^{-1} and depends on the composition, cross-linking percentage, and ionic strength of the immersion solution. Taguchi et al.[28] synthesized resorcinol−formaldehyde hydrogel with various resorcinol (R) (main monomer) and sodium carbonate (C) (reaction catalyst) ratios for cesium uptake. It was found that, when the R/C ratio (mol/mol) was 2.5, the diffusion coefficient was 1.45×10^{-12} m^2 s^{-1}, while with increase of the R/C ratio, the diffusion coefficient increased and reached 7.11×10^{-12} m^2 s^{-1}. Scally et al.[54] evaluated the diffusion coefficients of acrylamide monomer cross-linked with an agarose derivative (APA) hydrogel during Pb^{2+}, Ni^{2+}, Cd^{2+}, and Cu^{2+} removal. At metal ion concentrations of 10 ppm, the diffusion coefficients were found to be 8.0×10^{-10} m^2 s^{-1} for Pb^{2+}, 5.77×10^{-10} m^2 s^{-1} for Ni^{2+}, 6.09×10^{-10} m^2 s^{-1} for Cd^{2+}, and 4.41×10^{-10} m^2 s^{-1} for Ni^{2+}. Finally, the mean integral value of the fractal-based surface diffusivity is slightly greater for AAC with respect to SAC material. A deeper analysis of surface diffusivity

https://doi.org/10.1021/acs.iecr.2c00531
Ind. Eng. Chem. Res. 2022, 61, 8204−8219

parameters retrieved for the PVSDM-MBI reveals that for the same cation the fractional contribution of the fractal diffusion resistance (β parameter in eq 5) is similar for the two tested adsorbents. Moreover, the β value is more than 2-fold greater for Cs^+ with respect to Sr^{2+} for the same adsorbent. Additionally, the AAC sorbent displays greater values of both the hopping exponent α and the fractal exponent h for each adsorbate; for example, h is 2.5 and 1.5 times greater in the AAC case with respect to the SAC case for Cs^+ and Sr^{2+}, respectively. These results are also mirrored by stronger time-dependence of the surface diffusivity ratio $\frac{D_s(t)}{D_{s0}}$ for AAC adsorbent as depicted in Figure 6. It can be observed that all

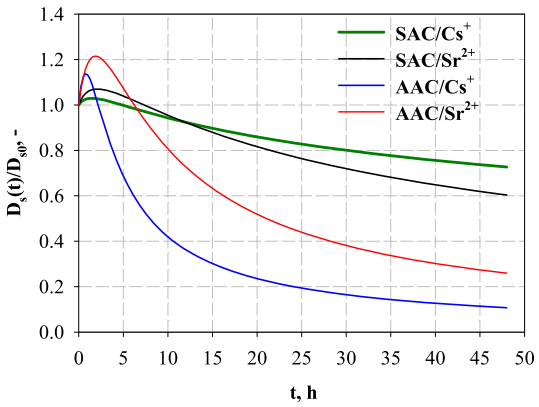

Figure 6. Surface diffusivity ratio as a function of time predicted by the PVSDM-MBI for the investigated sorbent/adsorbate systems.

systems under investigation exhibit a nonmonotonic pattern of $\frac{D_s(t)}{D_{s0}}$ with a maximum reached within the first 2.5 h, and the absolute values of the maxima are greater for AAC with respect to SAC cryogel. Moreover, the minimum values attained by the surface diffusivity ratio, i.e., under equilibrium conditions, are lower for AAC, which can be related to the greater values of h determined for this sorbent (which in turn affects the time decrease of the surface diffusivity): $\frac{D_s(t)}{D_{s0}}$ is 0.6 for SAC-Sr^{2+} and 0.1 for AAC-Cs^+ after 48 h. The analysis of the average Biot number shows that both external and internal resistances are important (with the internal one characterized by comparatively higher relevance) for AAC-Sr^{2+}, SAC-Cs^+, and SAC/Sr^{2+} systems ($\overline{Bi(t)}$ ranges from 14 to 20); however, $\overline{Bi(t)}$ is $O(10^2)$ for AAC-Cs^+, suggesting that in this case the intraparticle transport mechanism is significantly limiting with respect to the fluid film diffusion, linked to the remarkable greater value of k_f obtained for this system. Finally, a comparison of the values of surface diffusion and pores transport resistances through $\frac{\overline{D_s(t)}\rho_p\overline{q_0}}{D_p\overline{C_0}}$ values highlights that both intraparticle mechanisms are relevant (cf. also the discussion reported in Inglezakis et al.).[47]

3.5. Effect of Metal Ions Initial Concentration and Cryogels Loading on the Adsorption Isotherms. To evaluate the equilibrium behavior of the cryogels, three equilibrium adsorption isotherms were studied by using different experimental methods. The results are presented in Figure 7a–d. In the first and third set of experiments (experiments 1 and 3, cf. Table 2), various cryogel weights ranging from 0.0022 to 0.9 g were used at fixed concentration (100 or 1000 mg L^{-1}); this is a typical method for studying ion-exchange isotherms which require constant liquid phase normality.[55] The second set of isotherm experiments (experiment 2) was conducted under a fixed cryogel mass of 0.07 g

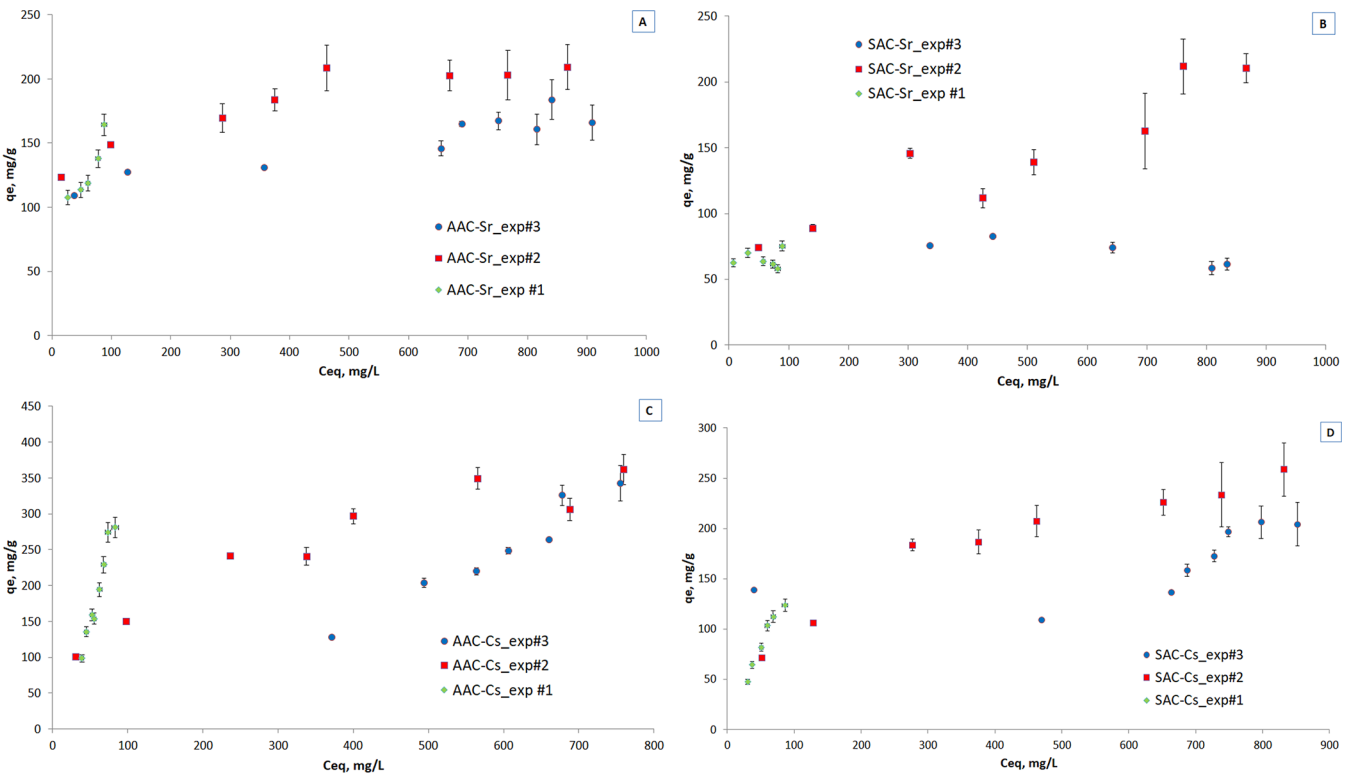

Figure 7. Isotherms of metal ions removal by cryogels: (a) AAC-Sr, (b) SAC-Sr, (c) AAC-Cs, and (d) SAC-Cs.

https://doi.org/10.1021/acs.iecr.2c00531
Ind. Eng. Chem. Res. 2022, 61, 8204–8219

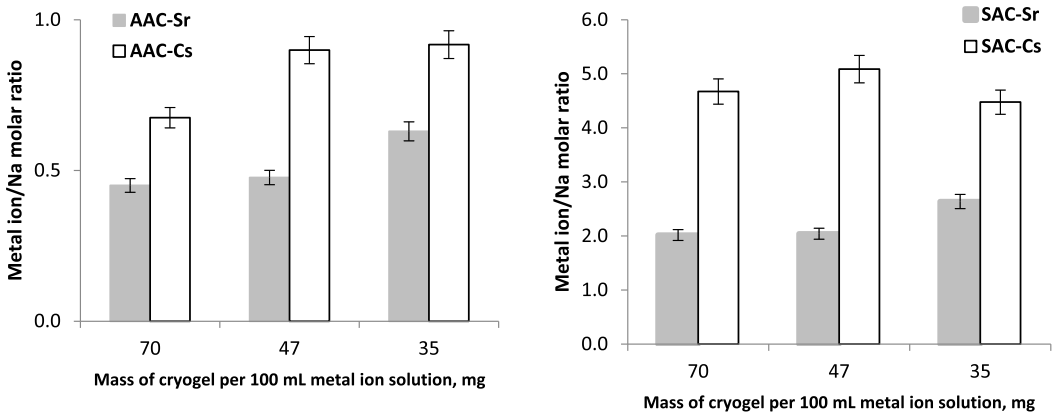

Figure 8. Molar ratio of removed metal ions to released Na^+ during adsorption as a function of the sorbent mass (metal ion solution volume of 100 mL).

and 100 mL of solution, with variable initial concentration ranging from 100 to 1000 mg L^{-1}. This is the standard method used in adsorption studies.

The results show that the equilibrium solid-phase concentration increases with the increase of initial concentration of metal ions in the solution, as expected. The maximum adsorption capacity of the AAC cryogel was 362 mg g^{-1} for Cs^+ and 209 mg g^{-1} for Sr^{2+}. The SAC polymer performed better at Cs^+ removal with respect to Sr^{2+}, with maximum adsorption capacities of 259 and 211 mg g^{-1}, respectively. In the adsorption literature, the derivation of isotherms is commonly carried out by varying the aqueous phase concentration while keeping the adsorbent mass to solution volume ratio constant. Interestingly, there are no studies comparing the standard method with alternatives, for instance, by varying the sorbent mass to solution volume ratio under constant aqueous phase concentration of adsorbate. If only adsorption takes place and at constant temperature, then the different experimental approaches must result in a single isotherm. However, in many systems, a combination of mechanisms exists, and such a comparison of methods becomes interesting. For instance, it is well-known that the isotherms of ion-exchange systems depend on total normality, a phenomenon called concentration-valence effect.[55] Taking into account that the removal mechanism of metals on cryogels is complex, being a combination of reversible adsorption, complexation, and ion-exchange processes, the differences among the isotherms derived by using different experimental procedures should emerge, a phenomenon that requires further investigation and is out of the scope of this paper.

Being the most common experimental method in sorption studies, the results of experiment 2 were used for isotherms modeling with Langmuir and Freundlich equations. From the outcomes of the adopted models (Table S2), it was found that the correlation coefficient (R^2) of the Freundlich isotherm model was higher than values obtained from Langmuir fitting for both cryogels in Sr^{2+} solutions. In the case of Cs^+ ions, both models showed high values of R^2 with slightly better performance for Freundlich in the case of AAC cryogel. These results indicate that both bivalent strontium and monovalent cesium ions can interact with various functional groups of polymers on the heterogeneous surface of the cryogels.

The maximum capacities achieved are comparable with those reported in the literature for 3D porous materials used for the removal of Sr^{2+} and Cs^+ from aqueous solutions. Garg et al.[20] synthesized a series of poly-*N*-vinyl imidazole-based hydrogels by adding four different cross-linkers for the removal of Sr^{2+} ions. The authors reveal that p(*N*-VIm-*cl*-DVB) hydrogel showed the best adsorption results with maximum capacity of 247 mg g^{-1} at pH 7.0. In another study, Choe and coauthors[21] fabricated an alginate/humic acid/Fe-amino clay hydrogel for targeted removal of Sr^{2+} ions under different conditions of pH, temperature, and competing cations. The result of the study showed that in a single-metal solution the synthesized hydrogel was able to remove up to 46 mg g^{-1} of Sr^{2+} ions, while from multicomponent model solution, it was able to remove only 8.3 mg g^{-1}.[21] In case of Cs^+ removal, many studies were done by use of Prussian blue modified polymers and clays. Zhao et al.[33] reported the production of PAMPS/PAAm hydrogel modified by $[Fe(CN)_6]$, and examined polymers composites capability to removal Cs^+ from 1000 ppm of CsCl solution at pH 7.0. The result showed the high uptake of cesium ions by coupling effect of Cs^+ with the framework of Prussian blue crystals and reached the maximum capacity of 420 mg g^{-1} of composite. In the studies of Bratskaya et al.,[27] macroporous Co^{2+}-chelated carboxyalkylchitosan cryogels were fabricated and modified with potassium ferrocyanide for selective capture of cesium ions. The results of the experiments showed that CEC/Co(II)$[Fe(CN)_6]$ cryogel was able to adsorb up to 132 mg g^{-1} of Cs^+ from 264 ppm solution at pH 3.0. More results on the removal of Sr^{2+} and Cs^+ from water by 3D polymeric adsorbents found in the literature are presented in Table S1.

3.6. Removal Mechanisms. The FT-IR analysis showed that some functional groups of cryogels can act as ion-exchangers and chelation agents toward cationic metals. The removal mechanisms proposed in our previous papers for Hg^{2+} and Cd^{2+} capture from aqueous solution may also be applied for Sr^{2+} and Cs^+ ions removal.[42,52] The mass of Na^+ released from cryogels was measured, and the Me/Na^+ (with Me = Sr^{2+} and Cs^+) molar ratio is shown in Figure 8 as a function of the mass of cryogel per fixed volume of metal ion solution. Ideally, if the ion exchange of Sr^{2+} occurs only with Na^+, then the molar ratio is 1:2, and for Cs^+, it is 1:1. In the case of AAC, the ratios are not far from the expected ones for ion exchange, and the deviations can be explained by the contribution of the functional groups. However, in the case of the SAC cryogel, for both target adsorbate ions, the Me/Na^+ ratio is much higher than the expected one for ion exchange, which means that the

https://doi.org/10.1021/acs.iecr.2c00531
Ind. Eng. Chem. Res. 2022, 61, 8204−8219

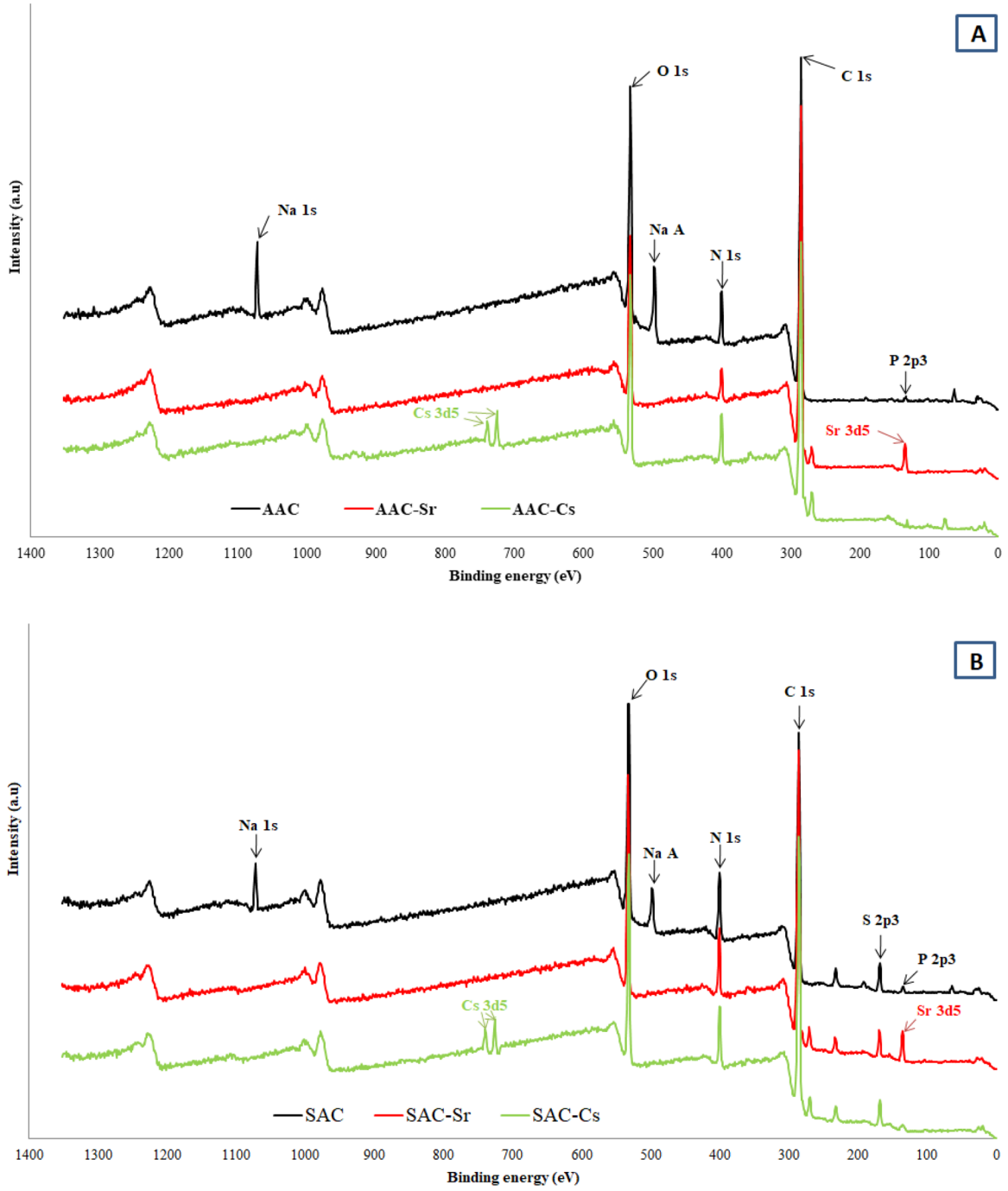

Figure 9. XPS patterns of cryogels before and after metal ions removal: (a) AAC and (b) SAC cryogels.

released amount of Na^+ is small. This happens due to the low initial concentration of sodium ions in the SAC cryogel (see section 3.1) and probably also because of the sulfonic acid's H^+, which might be exchanged for Sr^{2+} and Cs^+ cations.

The results of XPS characterization of cryogels before and after adsorption of the metal ions (Figure 9a,b) show that peaks of sodium ions Na 1s (~1071.4 eV) and Na Auger peak (~497.1 eV) of the parent AAC and SAC cryogels disappeared with the advent of corresponding metal ions peaks of strontium at 135.1 eV and cesium at 725.1 and 738.1 eV, indicating the relevance of the ion-exchange mechanism of sodium ions to selected cations. After the interaction of both cryogels with the studied cations, the binding energies of C−O (286.8 eV) and C═O (288.2 eV) are shifted by 0.7−1.2 eV to higher positions, due to the binding of positively charged metal ions.[56] Since most of the components for SAC are the same as those for AAC, the main difference is the presence of sulfonic acid groups in the structure of SAC cryogel. Figure 9b shows spectra of SAC cryogel before and after metal ions removal. The S 2p core level spectrum is deconvoluted into two major peaks centered at 167.5 and 169.0 eV, which are assigned to $2p_{3/2}$ and $2p_{1/2}$. These high oxidized states of sulfur are corresponding to sulfonic acid group ($-SO^{3-}$).[57] After interaction of metal ions, the sulfonic acid group peaks shifted of 0.5−0.7 eV to higher region, which suggests the formation of coordination bonds of sulfonic acid residues with cations.

https://doi.org/10.1021/acs.iecr.2c00531
Ind. Eng. Chem. Res. 2022, 61, 8204−8219

These findings indicate a combination of ion-exchange, adsorption, and chelation with the involvement of the carboxylic and sulfonic groups, resulting in the high adsorption capacity of the synthesized cryogels.

3.7. Leaching Experiments. AAC and SAC cryogels were immersed in water for 30 days (neutral pH) after Sr^{2+} and Cs^{+} adsorption, in order to verify undesired leaching phenomena. Results reported in Table 5 showed negligible leaching of Sr^{2+} metal ions, with values smaller than 1% for both cryogels. In the case of Cs^{+} ions, leaching was greater than that for strontium and reached 2.30 and 1.84% for AAC and SAC, respectively. Presumably, this phenomenon is associated with the monovalence of cesium and a weaker binding with functional groups of cryogels with respect to the strontium case.

Table 5. Leaching Results of Metal Ions from AAC and SAC Cryogels at pH 6.5[a]

adsorbent	total adsorbed metal ions [mg]	leached metal ion after 30 days [mg]	leached metal ion after 30 days [%]
AAC-Sr	8.89	0.0656	0.74
AAC-Cs	6.88	0.1585	2.30
SAC-Sr	4.45	0.0418	0.94
SAC-Cs	5.73	0.1054	1.84

[a]Experimental conditions: 0.07 g of sorbent in 100 mL of 100 mg L^{-1} metal ions solution.

3.8. Removal from Various Water Matrices and Comparison to Commercial Adsorbents. The results of Sr^{2+} and Cs^{+} removal from various water matrices and commercial adsorbents are presented in Table S3. The concentrations of coexisting cations in tap water were 77.3 ppm Na^{+}, 5.4 ppm K^{+}, 20.5 ppm Mg^{2+}, and 61.3 ppm Ca^{2+}, while in river water they were 19.7 ppm Na^{+}, 1.7 ppm K^{+}, 3 ppm Mg^{2+}, and 29 ppm Ca^{2+}.

In the case of Cs^{+} removal from UPW, in the first 30 min of experiment the zeolite and AAC sample removed around 53 and 37%, respectively, while the SAC adsorbed around 27%, and the ion-exchange resin removed only 5%. After 24 h of processing time, 86−87% of cesium ions were removed by commercial zeolite and AAC cryogel, and 60 and 39% were removed by SAC and ion-exchange resin, respectively. In tap and river water, due to the occurrence of coexisting cations, the removal effectiveness of all materials was lowered. However, the general pattern of removal was the same as that for UPW. After 24 h, the AAC cryogel and commercial zeolite were able to remove around 40 and 50% of Cs^{+} from tap water and 54 and 55% of Cs^{+} from river water, respectively, whereas the SAC sample and ion-exchange resin did not show any adsorption of cesium from tap water and only 21 and 27% from river water after 24 h of interaction, respectively.

As in the case of Cs, for the removal of Sr, commercial zeolite performs better in the first 30 min in all water matrices; however, the removal of strontium from UPW was higher and reached 66% in the first 30 min and more than 97% after 24 h. After 24 h in UPW, the AAC cryogel reached 95% removal of Sr^{2+}, while the SAC and the ion-exchange resin reached 80 and 36% removal. The tap water results showed that only SAC cryogel exhibited low effectiveness (around 27%), while the other ion-exchange materials showed 41−45% Sr^{2+} removal. The results of Sr^{2+} removal from river water followed the following ranking: commercial zeolite (64%) >AAC (50%) > SAC (49%) ≈ ion-exchange resin (49%).

3.9. Dynamic Adsorption Experiments. The cryogels were applied in a fixed-bed column for dynamic sorption, and results are reported in Figure 10. Data show that the breakthrough curve in the case of Cs is shifted toward longer times in comparison to Sr; for example, in the case of AAC cryogel, saturation occurs after about 35 and 20 min for Cs^{+} and Sr^{2+}, respectively. For the same cation, AAC displays better dynamic performance when compared to SAC cryogel. These results are in agreement with the kinetics (surface diffusivity) and equilibrium (capacity) results.

The breakthrough curves for the removal of the cryogels were modeled using the Thomas, Adams−Bohart, and Yoon−Nelson models, by applying linear regression analysis to determine the dynamic behaviors in the column. Comparisons of predicted model parameters together with values of experimental and theoretical adsorption capacity are shown in Table S4. Results show that that correlation coefficients for the Thomas and Yoon−Nelson models are practically equivalent and higher than values retrieved for the Adams−Bohart model. As an example, k_{Th} values are practically equivalent for AAC and SAC when considering Sr^{2+} adsorption, and at fixed adsorbent levels, the rate constant

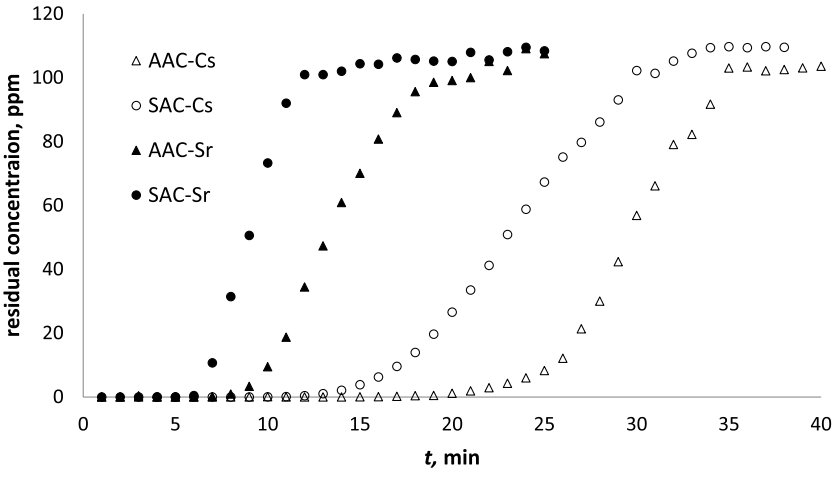

Figure 10. Breakthrough curves for AAC and SAC cryogels (adsorption of Cs^{+} and Sr^{2+}).

https://doi.org/10.1021/acs.iecr.2c00531
Ind. Eng. Chem. Res. 2022, 61, 8204−8219

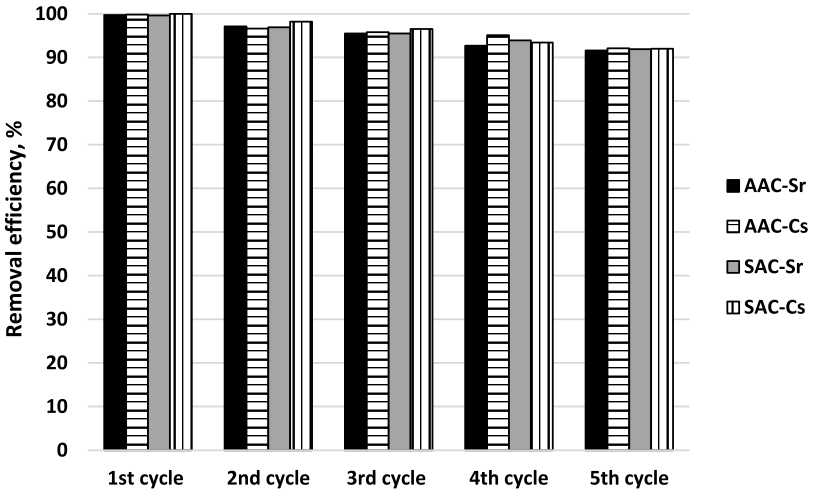

Figure 11. Removal efficiency of AAC and SAC cryogels for adsorption of Cs^+ and Sr^{2+} during five adsorption/desorption cycles.

values for strontium are slightly greater than figures retrieved for cesium.

3.10. Regeneration and Reusability of Cryogels. The recovery and reuse of the adsorbent for multiple cycles is one of the most important aspects from an economic point for industrial scale processes. Cryogel monoliths used in the column experiments were washed with 0.1 M HNO_3 and then by 0.1 NaOH and UPW. The removal efficiencies of cryogels toward Sr^{2+} and Cs^+ during five cycles are presented in Figure 11. After the first cycle of desorption/adsorption, the efficiencies of both cryogels were almost 100%. During the next cycles of regeneration and reuse, the adsorption behavior started to decrease and was found to be 96% for AAC-Sr, 97% for AAC-Cs, and 92 and 95% for Sr^{2+} and Cs^+ removed by the SAC cryogel, respectively. The removal efficiency decreased by 8% after five cycles, thus evidencing that the effectiveness of both cryogels was still high.

4. CONCLUSIONS

Two types of macroporous cryogels were studied toward Sr^{2+} and Cs^+ removal from aqueous solutions. The results demonstrated fast removal kinetics and high equilibrium capacities with the AAC cryogel being superior to the SAC cryogel. In particular, the adsorption capacity of the AAC cryogel reached 362 mg g^{-1} for Cs^+ and 209 mg g^{-1} for Sr^{2+}. In contrast, the SAC polymer was also better at Cs^+ removal, with a maximum capacity of 259 mg g^{-1}, while Sr^{2+} adsorption reached 211 mg g^{-1}. The combination of experimental, modeling, and characterization indicates that ion exchange followed by complexation reactions is the main mechanism of cations removal. Kinetics modeling by use of advanced diffusion-based equations showed that both external and internal resistances are important, and surface diffusivity displays a nonmonotonic pattern as predicted by a fractal-based expression. Column experiments demonstrated that the sorbents still retained more than 90% of their capacity after five adsorption/desorption cycles, which makes the cryogels very promising candidates for the scale-up of continuous adsorption units aimed at the removal of strontium and cesium from wastewaters.

ASSOCIATED CONTENT

Supporting Information

The Supporting Information is available free of charge at https://pubs.acs.org/doi/10.1021/acs.iecr.2c00531.

Adsorbents used in the literature for the removal of Cs^+ and Sr^{2+} ions from aqueous media, isotherms modeling results, residual concentrations of Cs^+ and Sr^{2+} in various water matrices after adsorption, breakthrough models parameters for adsorption of Cs^+ and Sr^{2+} onto cryogels, SEM/EDX mapping images of cryogels after adsorption of Sr^{2+} and Cs^+ metal ions, mathematical modeling for batch and column adsorption (PDF)

AUTHOR INFORMATION

Corresponding Authors

Vassilis J. Inglezakis − *Department of Chemical & Process Engineering, University of Strathclyde, Glasgow G1 1XJ, United Kingdom*; Email: vasileios.inglezakis@strath.ac.uk

Marco Balsamo − *Department of Chemical Sciences, University of Naples Federico II, Complesso Universitario di Monte Sant'Angelo, 80126 Napoli, Italy*; orcid.org/0000-0002-2063-8680; Email: marco.balsamo@unina.it

Authors

Alzhan Baimenov − *National Laboratory Astana, Nazarbayev University, Nur-Sultan 010000, Kazakhstan; Faculty of Chemistry and Chemical Technology, Al-Farabi Kazakh National University, Almaty 050012, Kazakhstan*

Fabio Montagnaro − *Department of Chemical Sciences, University of Naples Federico II, Complesso Universitario di Monte Sant'Angelo, 80126 Napoli, Italy*; orcid.org/0000-0002-6377-3989

Complete contact information is available at: https://pubs.acs.org/10.1021/acs.iecr.2c00531

Notes

The authors declare no competing financial interest.

NOMENCLATURE

$\overline{Bi(t)}$	average Biot number for PVSDM-MBI [−]
$C(t)$	adsorbate concentration at the fixed bed outlet at time t [mg m^{-3}]

https://doi.org/10.1021/acs.iecr.2c00531
Ind. Eng. Chem. Res. 2022, 61, 8204−8219

C_{eq} adsorbate concentration in the fluid bulk under equilibrium [mg m^{-3}]
C_0 adsorbate concentration at the fixed bed inlet [mg m^{-3}]
$C_p(t, r)$ free adsorbate local concentration in the sorbent pores (at time t) [mg m^{-3}]
$C_p(t, r)|_{r=R}$ free adsorbate local concentration (at time t) in the sorbent pores [mg m^{-3}] in correspondence of the solid external surface
$\overline{C(t)}$ average adsorbate concentration in the fluid bulk at time t [mg m^{-3}]
$\overline{C_0}$ average initial value of the adsorbate concentration in the fluid bulk [mg m^{-3}]
D_m molecular diffusion coefficient of adsorbate in water [m^2 s^{-1}]
D_p diffusion coefficient of adsorbate in the sorbent pores [m^2 s^{-1}]
D_s diffusion coefficient of adsorbate in the solid phase [m^2 s^{-1}]
D_{s0} zero-loading adsorbate surface diffusivity [m^2 s^{-1}]
$\overline{D_s(t)}$ mean integral value of the fractal-based surface diffusivity (eq 5) [m^2 s^{-1}]
F volumetric flow rate [m^3 s^{-1}]
H Heaviside function [−]
h fractal exponent [−]
k_{AB} Adams−Bohart's model rate constant [m^3 mg^{-1} s^{-1}]
K_F Freundlich's equilibrium adsorption constant [(mg g^{-1})(m^3 mg^{-1})$^{1/n}$]
k_f mass transfer coefficient in the fluid film [m s^{-1}]
K_H Henry's equilibrium adsorption constant [m^3 g^{-1}]
K_L Langmuir's equilibrium adsorption constant [m^3 mg^{-1}]
k_{Th} Thomas' model rate constant [m^3 mg^{-1} s^{-1}]
k_{YN} Yoon−Nelson's model rate constant [s^{-1}]
L fixed bed length [m]
m adsorbent mass [g]
N maximum ion adsorption capacity per unit volume of adsorbent column [mg m^{-3}]
n exponent in Freundlich's isotherm [−]
$q(t, r)$ adsorbate local concentration (at time t) in the adsorbed phase [mg g^{-1}]
q_{eq} equilibrium specific adsorption capacity [mg g^{-1}]
q_m specific adsorption capacity at saturation (monolayer) [mg g^{-1}]
q_0 maximum specific adsorption capacity [mg g^{-1}]
$\overline{q(t)}$ average specific adsorption capacity at time t [mg g^{-1}]
$\overline{q_0}$ adsorbate concentration in the solid, in equilibrium with $\overline{C_0}$ [mg g^{-1}]
R solid particle radius (swollen) [m]
r particle radial coordinate [m] R^2 coefficient of determination [−]
t time [s]
U_0 linear velocity of influent solution [m s^{-1}]
V solution volume [m^3]

Greek Symbols

α hopping exponent [−]
β fractional contribution of the fractal diffusion resistance [−]
ε_p particle porosity (swollen) [−]
θ surface coverage degree [−]
λ blockage parameter [−]
ρ_p particle density (swollen) [g m^{-3}]
τ time required for 50% adsorbate breakthrough [s]
τ_p particle tortuosity [−]

REFERENCES

(1) Mu, W.; Yu, Q.; Li, X.; Wei, H.; Jian, Y. Niobate Nanofibers for Simultaneous Adsorptive Removal of Radioactive Strontium and Iodine from Aqueous Solution. *J. Alloys Compd.* **2017**, *693*, 550−557.
(2) Moore, J. J.; Raine, T. P.; Jenkins, A.; Livens, F. R.; Law, K. A.; Morris, K.; Law, G. T. W.; Yeates, S. G. Decontamination of Caesium and Strontium from Stainless Steel Surfaces Using Hydrogels. *React. Funct. Polym.* **2019**, *142*, 7−14.
(3) Vardhan, K. H.; Kumar, P. S.; Panda, R. C. A Review on Heavy Metal Pollution, Toxicity and Remedial Measures: Current Trends and Future Perspectives. *J. Mol. Liq.* **2019**, *290*, 111197.
(4) Lee, I.; Park, C. W.; Yoon, S. S.; Yang, H.-M. Facile Synthesis of Copper Ferrocyanide-Embedded Magnetic Hydrogel Beads for the Enhanced Removal of Cesium from Water. *Chemosphere.* **2019**, *224*, 776−785.
(5) Atta, A. M.; Ismail, H. S.; Elsaaed, A. M. Application of Anionic Acrylamide-Based Hydrogels in the Removal of Heavy Metals from Waste Water. *J. Appl. Polym. Sci.* **2012**, *123*, 2500−2510.
(6) Çavuş, S.; Çakal, E. Poly(2-acrylamido-2-methyl-1-propane Sulfonic Acid-co-1-vinyl-2-pyrrolidone) Hydrogel and its Use in the Removal of Cd(II), Pb(II) and Cu(II). *Acta Phys. Polym. A* **2017**, *132*, 505−508.
(7) Matlock, M. M.; Howerton, B. S.; Atwood, D. A. Chemical Precipitation of Heavy Metals from Acid Mine Drainage. *Water Res.* **2002**, *36*, 4757−4764.
(8) Charerntanyarak, L. Heavy Metals Removal by Chemical Coagulation and Precipitation. *Water Sci. Technol.* **1999**, *39*, 135−138.
(9) Sunil, K.; Karunakaran, G.; Yadav, S.; Padaki, M.; Zadorozhnyy, V.; Pai, R. K. Al-Ti_2O_6 a Mixed Metal Oxide Based Composite Membrane: A Unique Membrane for Removal of Heavy Metals. *Chem. Eng. J.* **2018**, *348*, 678−684.
(10) Kang, S.-Y.; Lee, J.-U.; Moon, S.-H.; Kim, K.-W. Competitive Adsorption Characteristics of Co^{2+}, Ni^{2+}, and Cr^{3+} by IRN-77 Cation Exchange Resin in Synthesized Wastewater. *Chemosphere.* **2004**, *56*, 141−147.
(11) Sarwar, N.; Imran, M.; Shaheen, M. R.; Ishaque, W.; Kamran, M. A.; Matloob, A.; Rehim, A.; Hussain, S. Phytoremediation Strategies for Soils Contaminated with Heavy Metals: Modifications and Future Perspectives. *Chemosphere.* **2017**, *171*, 710−721.
(12) Da'na, E. Adsorption of Heavy Metals on Functionalized-Mesoporous Silica: A Review. *Microporous Mesoporous Mater.* **2017**, *247*, 145−157.
(13) Song, K.-C.; Lee, H. K.; Moon, H.; Lee, K. J. Simultaneous Removal of the Radiotoxic Nuclides Cs^{137} and I^{129} from Aqueous Solution. *Sep. Purif. Technol.* **1997**, *12*, 215−227.
(14) Hong, M.; Yu, L.; Wang, Y.; Zhang, J.; Chen, Z.; Dong, L.; Zan, Q.; Li, R. Heavy Metal Adsorption with Zeolites: The Role of Hierarchical Pore Architecture. *Chem. Eng. J.* **2019**, *359*, 363−372.
(15) Inglezakis, V. J.; Fyrillas, M. M.; Stylianou, M. A. Two-Phase Homogeneous Diffusion Model for the Fixed Bed Sorption of Heavy Metals on Natural Zeolites. *Microporous Mesoporous Mater.* **2018**, *266*, 164−176.
(16) Abdollahi, T.; Towfighi, J.; Rezaei-Vahidian, H. Sorption of Cesium and Strontium Ions by Natural Zeolite and Management of Produced Secondary Waste. *Environ. Technol. Innov.* **2020**, *17*, 100592.
(17) Liang, J.; Li, J.; Li, X.; Liu, K.; Wu, L.; Shan, G. The Sorption Behavior of CHA-Type Zeolite for Removing Radioactive Strontium from Aqueous Solutions. *Sep. Purif. Technol.* **2020**, *230*, 115874.
(18) Kaveeshwar, A. R.; Kumar, P. S.; Revellame, E. D.; Gang, D. D.; Zappi, M. E.; Subramaniam, R. Adsorption Properties and Mechanism of Barium (II) and Strontium (II) Removal from Fracking

https://doi.org/10.1021/acs.iecr.2c00531
Ind. Eng. Chem. Res. 2022, 61, 8204−8219

Wastewater using Pecan Shell Based Activated carbon. *J. Clean. Prod.* **2018**, *193*, 1−13.
(19) Chegrouche, S.; Mellah, A.; Barkat, M. Removal of Strontium from Aqueous Solutions by Adsorption onto Activated Carbon: Kinetic and Thermodynamic Studies. *Desalination.* **2009**, *235*, 306−318.
(20) Garg, G.; Chauhan, G. S.; Ahn, J.-H. Strontium(II) Ion Uptake on Poly(N-vinyl imidazole)-Based Hydrogels. *J. Appl. Polym. Sci.* **2012**, *124*, 3721−3727.
(21) Choe, S. R.; Haldorai, Y.; Jang, S.-C.; Rethinasabapathy, M.; Lee, Y.-C.; Han, Y.-K.; Jun, Y.-S.; Roh, C.; Huh, Y. S. Fabrication of Alginate/Humic Acid/Fe-Aminoclay Hydrogel Composed of a Grafted-Network for the Efficient Removal of Strontium Ions from Aqueous Solution. *Environ. Technol. Innov.* **2018**, *9*, 285−293.
(22) Yoon, J. Y.; Zhang, H.; Kim, Y. K.; Harbottle, D.; Lee, J. W. A High-Strength Polyvinyl Alcohol Hydrogel Membrane Crosslinked by Sulfosuccinic Acid for Strontium Removal via Filtration. *J. Environ. Chem. Eng.* **2019**, *7*, 102824.
(23) Khandaker, S.; Toyohara, Y.; Saha, G. C.; Awual, M. R.; Kuba, T. Development of Synthetic Zeolites from Bio-Slag for Cesium Adsorption: Kinetic, Isotherm and Thermodynamic Studies. *J. Water Process Eng.* **2020**, *33*, 101055.
(24) Khandaker, S.; Chowdhury, M. F.; Awual, M. R.; Islam, A.; Kuba, T. Efficient Cesium Encapsulation from Contaminated Water by Cellulosic Biomass Based Activated Wood Charcoal. *Chemosphere* **2021**, *262*, 127801.
(25) Parab, H.; Mahadik, P.; Sengupta, P.; Vishwanadh, B.; Kumar, S. D. A Comparative Study on Native and Gamma Irradiated Bentonite for Cesium Ion Uptake. *Prog. Nucl. Energy.* **2020**, *127*, 103419.
(26) Chen, S.; Hu, J.; Shi, J.; Wang, M.; Guo, Y.; Li, M.; Duo, J.; Deng, T. Composite Hydrogel Particles Encapsulated Ammonium Molybdophosphate for Efficiently Cesium Selective Removal and Enrichment from Wastewater. *J. Hazard. Mater.* **2019**, *371*, 694−704.
(27) Bratskaya, S.; Privar, Y.; Slobodyuk, A.; Shashura, D.; Marinin, D.; Mironenko, A.; Zheleznov, V.; Pestov, A. Cryogels of Carboxyalkylchitosans as a Universal Platform for the Fabrication of Composite Materials. *Carbohydr. Polym.* **2019**, *209*, 1−9.
(28) Taguchi, S.; Nakatani, T.; Saeki, H.; Tayakout-Fayolle, M.; Itoh, K.; Yamamoto, T. Characterization of Resorcinol−Formaldehyde Hydrogel as Adsorbent for Cesium Ion. *Adsorption* **2021**, *27*, 81−90.
(29) Cho, E.; Kim, J.; Park, C. W.; Lee, K.-W.; Lee, T. S. Chemically Bound Prussian Blue in Sodium Alginate Hydrogel for Enhanced Removal of Cs Ions. *J. Hazard. Mater.* **2018**, *360*, 243−249.
(30) Dwivedi, C.; Pathak, S. K.; Kumar, M.; Tripathi, S. C.; Bajaj, P. N. Potassium Cobalthexacyanoferrate-Gel Beads for Cesium Removal: Kinetics and Sorption Studies. *RSC Adv.* **2013**, *3*, 22102−22110.
(31) Wang, K.; Ma, H.; Pu, S.; Yan, C.; Wang, M.; Yu, J.; Wang, X.; Chu, W.; Zinchenko, A. Hybrid Porous Magnetic Bentonite-Chitosan Beads for Selective Removal of Radioactive Cesium in Water. *J. Hazard. Mater.* **2019**, *362*, 160−169.
(32) Taşdelen, B.; Osmanlioglu, A. E.; Kam, E. The Adsorption Behavior of Cesium on Poly(N-isopropylacrylamide/itaconic acid) Copolymeric Hydrogels. *Polym. Bull.* **2013**, *70*, 3041−3053.
(33) Zhao, P.; Zhang, W.; Kaneti, Y. V.; Azhar, A.; Alshehri, A. A.; Yamauchi, Y.; Hu, M. Confined Synthesis of Coordination Frameworks Inside Double-Network Hydrogel for Fabricating Hydrogel-Based Water Pipes with High Adsorption Capacity for Cesium Ions. *Bull. Chem. Soc. Jpn.* **2018**, *91*, 1357−1363.
(34) Baimenov, A.; Berillo, D. A.; Poulopoulos, S. G.; Inglezakis, V. J. A Review of Cryogels Synthesis, Characterization and Applications on the Removal of Heavy Metals from Aqueous Solutions. *Adv. Colloid Interface Sci.* **2020**, *276*, 102088.
(35) Onnby, L.; Giorgi, C.; Plieva, F. M.; Mattiasson, B. Removal of Heavy Metals from Water Effluents Using Supermacroporous Metal Chelating Cryogels. *Biotechnol. Prog.* **2010**, *26*, 1295−1302.
(36) Inglezakis, V. J.; Fyrillas, M. M.; Park, J. Variable Diffusivity Homogeneous Surface Diffusion Model and Analysis of Merits and Fallacies of Simplified Adsorption Kinetics Equations. *J. Hazard. Mater.* **2019**, *367*, 224−245.
(37) Inglezakis, V. J.; Fyrillas, M. M. Experimental Study of Zeolitic Diffusion by Use of a Concentration-Dependent Surface Diffusion Model. *Heliyon.* **2019**, *5*, e02143.
(38) Malakhova, I.; Golikov, A.; Azarova, Y.; Bratskaya, S. Extended Rate Constants Distribution (RCD) Model for Sorption in Heterogeneous Systems: 2. Importance of Diffusion Limitations for Sorption Kinetics on Cryogels in Batch. *Gels.* **2020**, *6*, 15.
(39) Inglezakis, V. J.; Balsamo, M.; Montagnaro, F. A Fractal-Based Correlation for Time-Dependent Surface Diffusivity in Porous Adsorbents. *Processes* **2020**, *8*, 689.
(40) Baimenov, A.; Berillo, D. A.; Inglezakis, V. J. Cryogel-Based Ag°/Ag_2O Nanocomposites for Iodide Removal from Water. *J. Mol. Liq.* **2020**, *299*, 112134.
(41) Baimenov, A.; Berillo, D.; Abylgazina, L.; Poulopoulos, S. G.; Inglezakis, V. J. Novel Amphoteric Cryogels for Cd^{2+} Ions Removal from Aqueous Solutions. *Key Eng. Mater.* **2018**, *775*, 376−382.
(42) Baimenov, A.; Berillo, D. A.; Azat, S.; Nurgozhin, T.; Inglezakis, V. J. Removal of Cd^{2+} from Water by Use of Super-Macroporous Cryogels and Comparison to Commercial Adsorbents. *Polymers (Basel)* **2020**, *12*, 2405.
(43) Ocampo-Pérez, R.; Leyva-Ramos, R.; Sanchez-Polo, M.; Rivera-Utrilla, J. Role of Pore Volume and Surface Diffusion in the Adsorption of Aromatic Compounds on Activated Carbon. *Adsorption* **2013**, *19*, 945−957.
(44) Chen, Y. D.; Yang, R. T. Concentration Dependence of Surface Diffusion and Zeolitic Diffusion. *AIChE J.* **1991**, *37*, 1579−1582.
(45) Montagnaro, F.; Balsamo, M. Deeper Insights into Fractal Concepts Applied to Liquid-Phase Adsorption Dynamics. *Fuel Process. Technol.* **2014**, *128*, 412−416.
(46) Balsamo, M.; Montagnaro, F. Fractal-Like Vermeulen Kinetic Equation for the Description of Diffusion-Controlled Adsorption Dynamics. *J. Phys. Chem. C* **2015**, *119*, 8781−8785.
(47) Inglezakis, V. J.; Balsamo, M.; Montagnaro, F. Liquid-Solid Mass Transfer in Adsorption Systems - An Overlooked Resistance? *Ind. Eng. Chem. Res.* **2020**, *59*, 22007−22016.
(48) Kadhim, M. J.; Gamaj, M. I. Estimation of the Diffusion Coefficient and Hydrodynamic Radius (Stokes Radius) for Inorganic Ions in Solution Depending on Molar Conductivity as Electro-Analytical Technique-A Review. *J. Chem. Rev.* **2020**, *2*, 182−188.
(49) Langmuir, I. The Constitution and Fundamental Properties of Solids and Liquids. PART I. Solids. *J. Am. Chem. Soc.* **1916**, *38*, 2221−2295.
(50) Masterova, M. N.; Andreyeva, L. I.; Zubov, V. P.; Polak, L. S.; Kabanov, V. A. Polymerization of Allylamines in the Presence of Protonic Acids. *Polym. Sci. U.S.S.R.* **1976**, *18*, 2234−2242.
(51) Kreindel', M. Y.; Andreyeva, L. I.; Kaplan, A. M.; Golubev, V. B.; Masterova, M. N.; Zubov, V. P.; Polak, L. S.; Kabanov, V. A. The Kinetics and Mechanism of the Low Temperature Post-Polymerization of Allylamine in the Presence of Phosphoric Acid. *Polym. Sci. U.S.S.R.* **1976**, *18*, 2553−2561.
(52) Baimenov, A.; Berillo, D. A.; Moustakas, K.; Inglezakis, V. J. Efficient Removal of Mercury (II) from Water by Use of Cryogels and Comparison to Commercial Adsorbents Under Environmentally Relevant Conditions. *J. Hazard. Mater.* **2020**, *399*, 123056.
(53) Berillo, D. Gold Nanoparticles Incorporated into Cryogel Walls for Efficient Nitrophenol Conversion. *J. Clean. Prod.* **2020**, *247*, 119089.
(54) Scally, S.; Davison, W.; Zhang, H. Diffusion Coefficients of Metals and Metal Complexes in Hydrogels Used in Diffusive Gradients in Thin Films. *Anal. Chim. Acta* **2006**, *558*, 222−229.
(55) Inglezakis, V. J.; Loizidou, M. D.; Grigoropoulou, H. P. Equilibrium and Kinetic Ion Exchange Studies of Pb^{2+}, Cr^{3+}, Fe^{3+} and Cu^{2+} on Natural Clinoptilolite. *Water Res.* **2002**, *36*, 2784−2792.
(56) Kim, Y.; Kim, Y. K.; Kim, S.; Harbottle, D.; Lee, J. W. Nanostructured Potassium Copper Hexacyanoferrate-Cellulose Hydrogel for Selective and Rapid Cesium Adsorption. *Chem. Eng. J.* **2017**, *313*, 1042−1050.

https://doi.org/10.1021/acs.iecr.2c00531
Ind. Eng. Chem. Res. 2022, 61, 8204−8219

(57) Nasef, M. M.; Saidi, H. Surface Studies of Radiation Grafted Sulfonic Acid Membranes: XPS and SEM Analysis. *Appl. Surf. Sci.* **2006**, *252*, 3073−3084.

https://doi.org/10.1021/acs.iecr.2c00531
Ind. Eng. Chem. Res. 2022, 61, 8204−8219